Atmos. Chem. Phys. Discuss., 9, 18985–19008, 2009
www.atmos-chem-phys-discuss.net/9/18985/2009/


Atmospheric Chemistry and Physics Discussions

This discussion paper is/has been under review for the journal *Atmospheric Chemistry and Physics (ACP)*. Please refer to the corresponding final paper in *ACP* if available.

# Impacts of electronically photo-excited $NO_2$ on air pollution control strategies in the South Coast Air Basin of California

**J. J. Ensberg**[1,*], **M. Carreras-Sospedra**[1], **and D. Dabdub**[1]

[1]Department of Mechanical and Aerospace Engineering, University of California at Irvine, Irvine, California, USA
[*]now at: The California Institute of Technology, Pasadena, California, USA

Received: 8 August 2009 – Accepted: 26 August 2009 – Published: 11 September 2009

Correspondence to: D. Dabdub (ddabdub@uci.edu)

Published by Copernicus Publications on behalf of the European Geosciences Union.





## Abstract

A new path for hydroxyl radical formation via photo-excitation of nitrogen dioxide ($NO_2$) and the reaction of photo-excited $NO_2$ with water is evaluated using the UCI-CIT model for the South Coast Air Basin of California (SoCAB). Two separate studies predict different reaction rates, which differ by nearly an order of magnitude, for the reaction of photo-excited $NO_2$ with water. Impacts of this new chemical mechanism on ozone and particulate matter formation, while utilizing both reaction rates, are quantified by simulating a two-day summer episode. In addition, sensitivity simulations are conducted to evaluate the uncertainty in the rate of reaction of photo-excited $NO_2$ with water reported in the literature. Results indicate that the addition of photo-excited $NO_2$ chemistry increases peak 1-h average ozone concentrations by up to 20.6%. Also, the new chemistry leads to moderate increases in particulate matter concentrations of up to 2.9%.

The importance of this new chemistry is then evaluated in the context of pollution control strategies. A series of simulations are conducted to generate isopleths for ozone and particulate matter concentrations, varying baseline nitrogen oxides ($NO_x$) and volatile organic compounds emissions. Results show that including $NO_2$ photo-excitation increases the sensitivity of ozone concentration to changes in $NO_x$ emissions. Namely, increasing $NO_x$ when $NO_2$ photo-excitation is included, while utilizing the higher reaction rate, leads to an increase in ozone concentration of up to 38.7% higher than a case without photo-excited $NO_2$. Ozone and particulate matter control strategies rely heavily on the variation of $NO_x$ and VOC emissions and the addition of the new chemical mechanism increases peak ozone and 24-h average PM concentrations in all locations under all $NO_x$ and VOC scaling factors while utilizing both reaction rates. Therefore, three-dimensional air quality models should be modified to include this new OH production mechanism, especially if used to develop emission controls strategies.




ACPD

9, 18985–19008, 2009



## 1 Introduction

The hydroxyl radical (OH) is one of the most important oxidants in the troposphere during daylight hours. It oxidizes volatile organic compounds (VOCs) and participates in the catalytic cycle of ozone formation. In remote areas, OH is produced via photolysis of ozone ($O_3$) in the presence of water. In polluted atmospheres, OH is also formed by the photolysis of nitrous acid (HONO) and hydrogen peroxide ($H_2O_2$). In addition, OH is formed through reaction of hydroperoxy radical ($HO_2$) and nitrous oxide. Hence, sources of $HO_2$ are eventual sources of OH. All these reactions have been long recognized as the major formation paths of OH and ozone.

$$O_3 + h\upsilon \rightarrow O(^1D) + O_2 \quad \text{(R1)}$$

$$O(^1D) + H_2O \rightarrow 2OH \quad \text{(R2)}$$

$$HONO + h\upsilon \rightarrow OH + NO \quad \text{(R3)}$$

$$H_2O_2 + h\upsilon \rightarrow 2OH \quad \text{(R4)}$$

$$HO_2 + NO \rightarrow NO_2 + OH \quad \text{(R5)}$$

where h is Planck's constant and is $\upsilon$ a photon of light with wavelength $\lambda$. A recent study by Li et al. (2008) suggested that an additional source of OH could contribute significantly to OH formation. The new OH production mechanism is as follows:

$$NO_2 + h\upsilon \rightarrow NO_2^* \quad \text{(R6)}$$

$$NO_2^* + H_2O \rightarrow HONO + OH \quad \text{(R7)}$$

$$NO_2^* + M \rightarrow NO_2 \quad \text{(R8)}$$

where $M$ is either an $O_2$ or $N_2$ molecule. Reaction (R6) occurs for nm. For nm, $NO_2$ dissociates into NO and $O(^3P)$. A previous study by Crowley and Carl (1997), analyzed



ACPD
9, 18985–19008, 2009



the yield of Reaction (R7), and suggested that this new mechanism has a limited impact on the OH formation. In contrast to these results, the study by Li et al. (2008) reported a reaction rate for Reaction (R7) to be an order of magnitude higher than that found by Crowley and Carl (1997). Despite the ambiguity as to the appropriate reaction rate to associate with Reaction (R7), both Li et al. (2008) and Crowley and Carl (1997) show that Reactions (R6–R8) have the potential to increase the amount of OH which is produced in the troposphere. Given the dependence of ozone production on OH concentrations in urban areas, the increase in OH due to Reaction (R7) must be considered when simulating ozone formation and formulating ozone control strategies.

Traditional control strategies for ozone focus on reducing NO and $NO_2$ (together known as $NO_x$) as well as VOC emissions. In conjunction with sunlight, OH, $NO_x$ and VOC mixing ratios play a key role in the amount of ozone that is produced throughout the day. Ozone control strategies are based on previous experimental and numerical studies and most, for the South Coast Air Basin of California (SoCAB), focus on reducing VOC emissions more aggressively than $NO_x$ emissions (Chock et al., 1999; Meng et al., 1997; Milford et al., 1994). Some studies that analyzed weekday to weekend differences in $NO_x$, VOC, and ozone levels suggest that in areas where $NO_x$ emissions are high, such as the SoCAB, decreasing $NO_x$ emissions may even have negative effects on peak ozone concentrations. This is due to the inability of the termination reaction of $NO_2$ with OH to produce nitric acid and remove OH from the system (Qin et al., 2004; Blanchard and Tanenbaum, 2003; Chinkin et al., 2003; Fujita et al., 2003). However, no study, to date, has included Reactions (R6–R8) into a three-dimensional air quality model to assess their impacts on emission control strategies.

The first objective of this study is to analyze the effect of including $NO_2$ photoexcitation processes in a three-dimensional air quality model. A statistical analysis is performed to quantify the improvement in air quality model performance due to the addition of the new chemistry. The second objective of this study is to determine how the addition of Reactions (R6–R8) affects potential air pollution control strategies. The results of this study demonstrate not only the positive effects $NO_2^*$ has on model ac-





curacy, but also show the impacts of $NO_2^*$ on current ozone control strategies and the direction future strategies should follow. Several statistical norms are presented to verify model accuracy and the validity of ozone concentration predictions.

## 2 Methodology

Three dimensional air-quality models have become the status quo for determining the impacts of newly discovered chemical reactions on pollution control strategies. Numerical simulations for this study are performed using the UCI-CIT Airshed Model (Harley et al., 1993). The UCI-CIT model was developed at the California Institute of Technology and continues to be upgraded by the Computational Environmental Sciences Laboratory (CESLab) at the University of California, Irvine. The modeling domain used for this study is presented in Fig. 1.

### 2.1 Model evaluation for new chemical mechanism

The scientific literature reports two different reaction rates associated with Reaction (R7), which are shown in Table 1. Therefore, this study explores the impacts of both reaction rates on ozone formation. Three simulated cases are compared to meteorological and air quality data measured by the California Air Resources Board (ARB) on 27–28 August 1987. Data were collected as part of the Southern California Air Quality Study (SCAQS) and have been used extensively to validate air quality models in other studies (Meng et al., 1998; Griffin et al., 2002). In addition, Zeldin et al. (1990) indicated that 28 August 1987 is representative of the meteorological conditions in the South Coast Air Basin of California, which makes it suitable for modeling an air quality episode. Hence, meteorological and air quality data for 27–28 August are used as the basis for the assessment of the impact of the photo-excitation processes on ozone and particulate matter control dynamics.

The three simulated cases include: (i) the UCI-CIT Airshed Model's base case, which



ACPD
9, 18985–19008, 2009



do not include Reactions (R6–R8), (ii) a case which includes the new chemistry while utilizing Li et al.'s high reaction rate for Reaction (R7), hence referred to as the "high reaction rate case", and (iii) a case which includes the new chemistry while utilizing Crowley and Carl's low reaction rate case for Reaction (R7), hence referred to as the "low reaction rate case". The three simulated cases are summarized in Table 1.

Model performance for the three cases is evaluated using the following statistical norms, as described by Russell and Dennis (2000), which were used previously to assess the performance of the UCI-CIT Airshed Model and its representation of secondary organic aerosols (Griffin et al., 2002):

Normalized bias, D

$$D = \frac{1}{N}\sum_{i=1}^{N}\frac{(C_p(x_i,t) - C_o(x_i,t))}{C_o(x_i,t)}, \quad t = 1,24. \tag{1}$$

Gross error, $E_d$ (for hourly observed values of $O_3$>60 ppb)

$$E_d = \frac{1}{N}\sum_{i=1}^{N}\frac{|C_p(x_i,t) - C_o(x_i,t)|}{C_o(x_i,t)}, \quad t = 1,24. \tag{2}$$

Unpaired peak prediction accuracy, $A_u$

$$A_u = \frac{C_p(x,t)_{\max} - C_o(x',t')_{\max}}{C_o(x',t')_{\max}} \times 100\%. \tag{3}$$

Total Unpaired peak prediction accuracy, $A_u$

$$A_{u,\text{total}} = \frac{1}{N}\sum_{i=1}^{N}\frac{C_p(x,t)_{\max,i} - C_o(x',t')_{\max,i}}{C_o(x',t')_{\max,i}} \times 100\%. \tag{4}$$

where $N$ is the number of monitoring stations, $x_i$ is the location of the monitoring station $i$, $C_o(x_i,t)$ is the observed value at monitoring station $i$ for hour $t$, $C_p(x_i,t)$ is the predicted value at monitoring station $i$ for hour $t$, $C_o(x',t')_{\max}$ is the maximum 1 h observed concentration over all hours and monitoring stations, $C_p(x,t)_{\max}$ and is the





maximum 1 h predicted concentrations over all hours and surface cells. The statistical analysis is based on the measured values by the air quality monitoring network existing during that episode, which included 30 monitoring stations.

### 2.2 Evaluation of emission control strategies

Previous studies have attempted to quantify the effects of altering $NO_x$ and VOC emission scaling factors on the formation of aerosol pollutants and the reduction of ozone (Winner et al., 1995; Meng et al., 1997; Nguyen and Dabdub, 2002). In this study, multiple day summer smog episodes are simulated while accounting for all feasible combinations of $NO_x$ and VOC emission ratios. In all three cases, the emissions of $NO_x$ and VOC emissions are amplified by factors of 0.0, 0.4, 0.8, 1.0, 1.2, 1.6, 2.0, throughout the domain of the model. Pollutants are calculated for each combination of $NO_x$ and VOC emission scaling factors, which results in 49 emission profiles per case. Simulation results are illustrated in isopleth charts to illustrate the dynamics of emission reductions. This study focuses on isopleths constructed for each of the three cases using the peak ozone concentration and 24-h average $PM_{10}$ concentration at selected locations. The impact of the new chemistry on emission control strategies is then evaluated by calculating the difference between isopleths resulting from including Reactions (R6–R8) at specific locations and the base case.

## 3 Results

### 3.1 Baseline air quality simulations

To reduce the effects of initial conditions on final concentrations, 27 and 28 August are first simulated excluding any aerosol phase chemistry. The final concentrations after these two days are then used as initial conditions for the same two day simulation with aerosol phase chemistry included in the simulation. Previous studies have shown that



ACPD
9, 18985–19008, 2009





this technique reduces irregularities caused by initial conditions up to 90% after 2 days of simulation (Nguyen and Dabdub, 2002).

Since $NO_2$ photolyzes throughout the day to produce NO, it is important to analyze $NO_2$ and NO separately and not as $NO_x$. Figure 2a–c shows the 1-h NO concentrations, resulting from the simulated cases together with measured concentrations in the cities of Los Angeles, Pomona, and Riverside for 27–28 August, 1987. Figure 2d–f shows the simulated and measured 1-h average ozone concentrations for the same cities and period of time. Simulated results shown in Fig. 2 correspond to the three cases described above. The corresponding $NO_2$ concentration plots (not shown) also present substantial increases of peak $NO_2$ concentrations which are also amplified by the use of the high reaction rate as opposed to the low reaction rate. This is due to $NO_2$ molecules which become excited, but do not react with $H_2O$, and later become quenched during peak concentration hours.

The incorporation of Reactions (R6–R8) results in a decrease in NO for Riverside throughout the two-day simulation. The maximum decrease in NO is 20 ppb, which occurs at hour 30 in the high reaction rate case. Similar trends in NO decreases occur in Los Angeles, although the differences are considerably smaller, with maximum decreases in NO concentrations less than 1–2 ppb. Pomona also exhibits similar trends in NO reduction with the inclusion of Reactions (R6–R8). The maximum decrease results at hour 41 and is close to 10 ppb. These decreases are due to the inability of $NO_2^*$ to dissociate into NO and $O(^3P)$ until it is quenched to its ground-state, $NO_2$, by either $O_2$ or $N_2$. This observation is further confirmed by the decreases in NO being larger for the high reaction rate case than for the low reaction rate case.

Ozone is one of the main pollutants of interest, and the resulting increases in ozone concentrations presented in Fig. 2d–f merit significant attention. In Los Angeles, Fig. 2d, the second simulated peak concentration, for both simulated cases are much lower than the measured values. However, the maximum increases in simulated ozone concentration due to Reactions (R6–R8) still occur at the peaks and are equal to 20 ppb. Measured ozone concentrations in Pomona, Fig. 2e, during the first



ACPD
9, 18985–19008, 2009



peak are close to 100 ppb higher than any predicted concentrations. The maximum differences between simulated concentrations and measured concentrations during the second peak decrease to 50 ppb, although there is a much stronger similarity in shape among all four cases. Similar trends in ozone increases occur in Riverside, Fig. 2f. By including Reactions (R6–R8) into the simulation, an increase in ozone production occurs during all daylight hours. The high reaction rate results in the largest increases in ozone, with the maximum differences being approximately 10 ppb and occurring at the two peaks (hour 16 and hour 39). Although the simulated peak concentrations are significantly less than the measured peak concentrations at this location, there is still much overlap in the shape between all four cases throughout the 48 h simulation.

The model performance results for the base case and the cases with the addition of Reactions (R6–R8) are summarized in Table 2. Total normalized error and bias in the low reaction rate case decrease by 0.1% and 1.2%, respectively, in relation to the base case. Total normalized error and bias in the high reaction rate case decrease by 0.5% and 2.0%, respectively, in relation to the base case. The most substantial improvement in the UCI-CIT Airshed Model performance occurs for its total unpaired peak predictions of ozone concentrations. This norm shows that the predicted peak ozone concentrations become substantially closer to the measured peak ozone concentrations at each measuring location. Note that positive errors cancel negative errors when matching peak predictions with measured concentrations using the total unpaired peak prediction norm. This statistical measure is quite significant when formulating ozone control strategies because if peak concentrations are within acceptable limits, then concentrations at other hours will be consequently within acceptable limits.

### 3.2 Impacts of excited nitrogen dioxide on ozone control strategies

Los Angeles and Riverside have been the focus of several studies due to their notoriously poor air quality and high levels of $NO_x$ and VOC emissions. Due to its location between Los Angeles and Riverside, Pomona has also been included in this study to better understand the evolution of pollution formation in the downwind direction.



ACPD
9, 18985–19008, 2009



Isopleths created using peak ozone concentrations in Los Angeles are considerably different than those for Riverside. This is primarily due to the differences in emissions between the two cities.

The resulting peak 1-h average ozone isopleths for Los Angeles are shown in Fig. 3a–c. Figure 3b shows the differences in ozone concentrations in Los Angeles between the low reaction rate case and the base case, whereas Fig. 3c presents the differences between the high reaction rate case and the base case. Although the two figures have somewhat similar shapes, the high reaction rate case results in much larger increases in ozone concentrations (12–15 ppb). The largest peak 1-h average ozone concentration in Fig. 3a occurs at VOC factor equal to 2 and $NO_x$ factor equal to 0.4. However, the differences in peak ozone concentrations due to Reactions (R6–R8) steadily increase with increasing VOC factors, but reach a maximum increase at $NO_x$ equal to 1.2, and then begin to decrease. The existence of this maximum illustrates the change from $NO_x$-limited conditions to VOC-limited conditions, which is determined by the VOC to $NO_x$ ratio present in that particular location. The importance of VOC to $NO_x$ ratios, which relates ozone sensitivity to $NO_x$ and VOC emission changes, is discussed in the following section. The inclusion of Reactions (R6–R8) not only results in an ~8% increase in peak ozone concentrations, but also causes the increase to occur in an isopleth regime – pair of VOC and $NO_x$ emissions scaling factors – that does not coincide with peak ozone concentrations in the base case as shown in Fig. 3a. The differences between peak ozone concentrations in cases with and without the new chemistry distort the shape of the isopleths in the high and low reaction rate cases with respect to the base case, suggesting the need for re-evaluation of the dynamics of ozone and particulate matter control strategies.

The evaluation of isopleths based on Los Angeles alone merits reconsidering how aggressively $NO_x$ and VOC emissions should be controlled to reduce peak ozone concentrations. This is further confirmed by evaluating results in Pomona and Riverside. Pomona is the location for which peak ozone concentrations in the high and low reaction rate cases differ the most. Figure 3d shows the isopleths composed of the peak





ozone concentrations in Pomona for the base case. Figure 3e presents the differences in ozone concentration between the low reaction rate case and the base case, and it indicates that the greatest increase in ozone (8 ppb) due to Reactions (R6–R8) occurs at $NO_x$ equal to 0.5 and VOC equal to 2.0. Conversely, Fig. 3f indicates that the increase in ozone due to the high reaction rate scales nearly equal with increasing $NO_x$ and VOC factors. The largest increase in ozone for the high reaction rate case in Pomona is 25 ppb and occurs at $NO_x$ equal to 2 and VOC equal to 2. Therefore, Pomona illustrates the necessity to clarify what reaction rate should be used in Reaction (R7). Instead of the variations in peak ozone concentrations being a function only of whether or not Reactions (R6–R8) are included in the UCI-CIT model, as is the case in Los Angeles and Riverside, they are now strongly a function of which reaction rate is used. Given the increased accuracy of the model in the high reaction rate case, it is believed that the differences present in Fig. 3f should be used more extensively when formulating ozone control strategies.

The resulting peak 1-h average ozone isopleths for Riverside are shown in Fig. 3g–i. Figure 3g shows the peak 1-h average ozone concentrations for the base case conditions, whereas Fig. 3h–i show the difference between the base case and the low and high reaction rate case, respectively. By including Reactions (R6–R8), Fig. 3h shows increases of 1–2 ppb for most of the grid. There is a small region, centered at $NO_x$ equal to 0.8 and VOC equal to 1.6, which results in increases between 2–4 ppb. The differences present in Fig. 3h are negligible when compared to the base case concentrations (~0.8%). Figure 3i, which corresponds to the high reaction rate, shows significantly larger differences in ozone production. The peak ozone concentrations steadily increase with increasing $NO_x$ and VOC. Ozone concentrations increase by up to 18 ppb and these increases occur in the region above $NO_x$ equal to 1.2 and VOC equal to 0.6.



ACPD
9, 18985–19008, 2009



### 3.3 Importance of VOC/$NO_x$ Ratio

Ozone control strategies rely primarily on the variation of $NO_x$ and VOC emissions to abate ozone production. OH reacts with both $NO_x$ and VOC which is directly emitted or transported from upwind, to produce ozone. The ratio of VOC to $NO_x$ determines which process is likely to be initiated by an OH molecule. At high VOC to $NO_x$ ratios, OH primarily reacts with VOC which enhances the formation of ozone. At low VOC to $NO_x$ ratios, the reactions between $NO_x$ and OH dominate, which is a termination reaction for ozone formation.

$$OH + NO_2 + M \rightarrow HNO_3 + M\,. \quad \text{(R9)}$$

There is a specific VOC to $NO_2$ ratio above which Reaction (R9) results in the termination of OH and $NO_2$ from the system, which decreases the rate of ozone production. Seinfeld and Pandis (2006) examined a simplified mechanism and found this ratio to be 5.5 to 1. Results indicate that the transitional VOC to $NO_x$ ratio for the UCI-CIT Airshed Model is closer to 15 to 1. Therefore, below this limit, increasing $NO_x$ emissions results in the removal of OH from the system and the overall decrease in ozone production. In addition, $NO_x$ acts as a sink for ozone through direct titration (Reaction R10).

$$NO + O_3 \rightarrow O_2 + NO_2\,. \quad \text{(R10)}$$

In the South Coast Air Basin of California, baseline $NO_x$ emissions are generally high, providing atmospheric conditions under low VOC to $NO_x$ ratios. Under these conditions, decreasing $NO_x$ alone leads to increases in ozone concentrations. For instance, it is well recognized that a major cause for having statistically higher ozone concentrations of ozone during the weekends in the South Coast Air Basin of California is the lower emissions of $NO_x$ with respect to weekdays, which reduces the yield of Reactions (R9–R10) (Qin et al., 2004; Blanchard and Tanenbaum, 2003; Chinkin et al., 2003; Fujita et al., 2003). The isopleths presented in Fig. 3a, d and g show that a decrease in $NO_x$ emissions of over 80% are necessary to achieve any decrease in



ACPD
9, 18985–19008, 2009



ozone concentration, whereas moderate decreases in VOC emissions alone reduce ozone concentrations immediately. In general, the higher the emissions of $NO_x$, and the lower VOC to $NO_x$ ratios, the more difficult is to reduce ozone by controlling $NO_x$ emissions alone. For example, in Los Angeles, with total $NO_x$ emissions of up to 6.59 t/day and VOC/$NO_x$ equal to 6.79, a reduction in $NO_x$ emissions of 60% would increase ozone concentration by 244%. Total $NO_x$ emissions in Pomona and Riverside are 1.57 t/day and 1.02 t/day, and respective VOC to $NO_x$ ratios are 7.71 and 11.5. A decrease in $NO_x$ emissions of 60% in Pomona results in a 41.1% increase in ozone concentrations, whereas the same decrease will result in an 8.29% decrease in ozone concentrations in Riverside.

The incorporation of Reactions (R6–R8) increases peak ozone concentrations in all locations under all $NO_x$ and VOC scaling factors. The increases in ozone concentrations occur because the mechanism inactivates a molecule of $NO_2$ through photo-excitation, that otherwise could react with OH and would terminate the ozone production. The OH produced by the reaction of photo-excited $NO_2$ with water can then participate in the oxidation of another VOC molecule, increasing ozone production. This deactivation of $NO_2$ increases the effective VOC to $NO_x$ ratio, and as a result, ozone increases in greater extent than if photo-excitation of $NO_2$ is not included. However, the extent of the ozone increases due to the new mechanism varies from location to location, as a function of the baseline $NO_x$ emissions and the resulting VOC to $NO_x$ ratios. This variability in the impacts of $NO_2$ photo-excitation is more evident in the high reaction rate case.

As shown in Fig. 3c, in Los Angeles, the maximum increases in ozone concentration occur at $NO_x$ scaling factors of 1–1.2. At higher $NO_x$ scaling factors, the contribution of $NO_2$ photo-excitation to ozone production diminishes because the overall ozone formation is limited by the high emissions and the low VOC to $NO_x$ ratios. Conversely, in Pomona and Riverside, the contribution of $NO_2$ photo-excitation to ozone formation increases with the increase in $NO_x$ scaling factors (Fig. 3f and i), because in these locations VOC to $NO_x$ ratios are higher than in Los Angeles. As a result, the increase



ACPD
9, 18985–19008, 2009



in ozone production due to the new mechanism is not offset by the high level of $NO_x$ emissions, and hence, ozone concentrations in the high reaction rate case increase with respect to the base case, as the scaling factor for $NO_x$ increases. It should be noted that the increases in ozone concentration in Riverside tend to occur at higher $NO_x$ scaling factors and lower VOC scaling factors than in Pomona, because VOC to $NO_x$ ratio is higher in Riverside. Despite both areas having comparable emissions, the VOC to $NO_x$ ratio in Riverside is significantly higher than in Pomona. These differences are attributed to upwind concentrations. Pomona, which is downwind from Los Angeles, is affected by the upwind high $NO_x$ levels that limit the formation of ozone at high $NO_x$ scaling factors. On the other hand, Riverside is farther downwind from Pomona, which lowers the sensitivity to $NO_x$ emissions from Los Angeles.

### 3.4 Impacts of excited nitrogen dioxide on PM concentrations

Although ozone control strategies are the main consideration of this study, there are several other pollutants whose production is strongly connected to ozone production. These pollutants, such as particulate matter whose diameter is less than 10 µm ($PM_{10}$) and particulate matter whose diameter is less than 2.5 µm ($PM_{10}$), are strongly affected by including Reactions (R6–R8) into the UCI-CIT model. Figure 3j shows isopleths of the 24-h average concentrations of $PM_{10}$ in Riverside for the base case on 28 August, 1987. As discussed by Nguyen and Dabdub (2002), in the regime of low $NO_x$ scaling factors, formation of secondary particles increases linearly with the increase in $NO_x$ emissions. This increase is tightly related to the increase in ozone concentration shown in Fig. 3g. Increasing ozone concentration increases the formation of OH, via Reactions (R1–R2), which in turn can react with $NO_2$ to form nitric acid which eventually produces aerosols via Reaction (R11):

$$HNO_3(g) + NH_3(g) \rightleftharpoons NH_4NO_3(p)\,. \qquad \text{(R11)}$$

Under a regime of high $NO_x$ and low VOC scaling factors, $NO_x$ ends up removing $O_3$, and hence, reduce OH and aerosol formation. At high $NO_x$ and VOC scaling factors,




ozone concentrations are the highest, producing high levels of OH and particles. In addition, in this regime of high $NO_x$ and VOC, formation of particles also has significant contributions from the formation of $N_2O_5$ at night by the reaction of ozone with $NO_x$ (as suggested by Nguyen and Dabdub, 2002). $N_2O_5$ can then react with water to form nitric acid, which leads to the formation of particles.

As with ozone, the low reaction rate case results in small (~1.0%) increases in peak 1-h average $PM_{10}$ concentrations for all $NO_x$ and VOC scaling factors. Figure 3k shows a complementary relationship between $NO_x$ and VOC emission scaling factors which causes $PM_{10}$ to increase at high $NO_x$ and low VOC as well as low $NO_x$ and high VOC. The largest increase in $PM_{10}$ concentrations occur for $NO_x$ and VOC factors equal to 2.0 and are equal to 1.4%.

In the high reaction rate case (see Fig. 3l), the addition of Reactions (R6–R8) leads to increases in 24-h average $PM_{10}$ concentrations of up to 8.0%. Also, the differences in $PM_{10}$ concentrations are almost entirely dependent on $NO_x$ scaling factors below 1.8. There are two main mechanisms that explain this behavior. First, the increase in $NO_x$ increases the potential formation of photo-excited $NO_2$, which can then form OH molecules that will end up forming aerosols. Second, particulate matter formation is tightly related to ozone, as more ozone photolyzes during the day to produce OH, or it reacts with $NO_x$ at night to produce $N_2O_5$.

Previously, Nguyen and Dabdub (2002) found that $PM_{10}$ formation in the SoCAB is significantly more sensitive to changes in ammonia emissions than to either VOC or $NO_x$ emissions. The results presented in this article, however, suggest that the addition of $NO_2$ photo-excitation could increase the sensitivity of particle formation to changes in $NO_x$ emissions. Namely, a decrease in $NO_x$ emissions would achieve a higher decrease in particle formation if photo-excitation of $NO_2$ were included. Therefore, Reactions (R6–R8) merit consideration for air quality models not only for the assessment of ozone formation, but also for the potential impacts of this mechanism in the formation of secondary particulate matter.





## 4 Conclusions

This study is the first to incorporate a new alternative path of hydroxyl radical formation via electronic photo-excitation of $NO_2$ into the chemical mechanism of a three dimensional air quality model. This study includes the analysis of uncertainty associated with the reaction rate of electronically excited $NO_2$ with water to form OH, based on studies performed by Li et al. (2008) and Crowley and Carl (1997). Results are used to assess the effects of the new mechanism on model accuracy and its impacts on ozone control strategies in the South Coast Air Basin of California.

The sensitivity of ozone and particulate matter formation to the new chemical path are quantified by simulating a two-day summer episode. The resulting simulated concentrations for the high reaction rate case (based on Li et al. 2008), the low reaction rate case (based on Crowley and Carl, 1997), and the UCI-CIT base case are then compared statistically to measured concentrations. Results indicate the largest impacts of $NO_2$ photo-excitation on ozone concentrations occur at the peaks for all cases. Results also show that model predictions of peak ozone concentrations improve upon including the new chemical mechanism into the UCI-CIT model. In particular, substantial improvements occur for peak ozone predictions at each location in the high reaction rate case.

Results of emission control strategies indicate that the impacts of $NO_2$ photo-excitation are most evident in the high reaction rate case. In areas with high $NO_x$ emissions and low VOC to $NO_x$ ratios, such as Los Angeles, the highest increases in peak ozone concentrations due to the new mechanism occur for moderate increases of $NO_x$ emissions. In downwind cities with low $NO_x$ emissions and high VOC to $NO_x$ ratios, such as Pomona and Riverside, the impacts of the new chemical mechanism are strongest with high $NO_x$ emissions. Ozone concentrations in these three locations experience little change in sensitivity to VOC emissions. Moderate increases in 24-h average $PM_{10}$ concentrations result in the high reaction rate case. Also, at $NO_x$ scaling factors below 1.8, the differences in $PM_{10}$ concentrations are almost entirely independent of VOC scaling factors. The results presented in this article suggest that the ad-





dition of $NO_2$ photo-excitation increases the sensitivity of ozone and particle formation to changes in $NO_x$ emissions above that which previous studies report.

Ozone and particulate matter control strategies rely heavily on the variation of $NO_x$ and VOC emissions and the addition of the new chemical mechanism increases peak ozone concentrations in all locations under all $NO_x$ and VOC scaling factors while utilizing both reaction rates. Therefore, three-dimensional air quality models should be modified to include this new OH production path. The UCI-CIT air quality model's ability to predict accurately ozone and particulate matter formation in urban areas depend largely on which reaction rate is used in the new chemical mechanism. Based on model performance, strategies deduced from the high reaction rate case results should be used more extensively when formulating ozone and particulate matter control strategies. However, there is still a large uncertainty as to what the true reaction rate is. Consequently, further experimental work must be conducted to reduce uncertainty in the reaction rate of Reaction (R7).

*Acknowledgements.* The authors would like to thank the Undergraduate Research Opportunities Program (UROP) at the University of California at Irvine for their support with this research project.

## References

Blanchard, C. L. and Tanenbaum, S. J.: Differences between weekday and weekend air pollutant levels in southern California, J. Air Waste Manage., 53, 816–828, 2003.

California Air Resources Board: Air Quality Data Statistics. Aerometric Data Analysis and Management system, http://www.arb.ca.gov/adam/welcome.html, last accessed 2008.

Chinkin, L. R., Coe, D. L., Funk, T., Hafner, H., Roberts, P., Ryan, P., and Lawson, D.: Weekday versus weekend activity patterns for ozone precursor emissions in California's South Coast Air Basin, J. Air Waste Manage., 53, 829–843, 2003.

Chock, D. P., Chang, T. Y., Winkler, S. L., and Nance, B. L.: The impact of an 8 h air quality standard on ROG and $NO_x$ controls in Southern California, Atmos. Environ., 33, 2471–2485, 1999.





Crowley, J. N. and Carl, S. A.: OH formation in the photoexcitation of $NO_2$ beyond the dissociation threshold in the presence of water vapor, J. Phys. Chem., 101, 4178–4184, 1997.
Fujita, E. M., Stockwell, W. R., Campbell, D. E., Keislar, R. E., and Lawson, D. R.: Evolution of the magnitude and spatial extent of the weekend ozone effect in California's South Coast Air Basin,1981–2000, J. Air Waste Manage., 53, 802–815, 2003.
Griffin, R. J., Dabdub, D., and Seinfeld, J. H.: Secondary organic aerosol, 1. Atmospheric chemical mechanism for production of molecular constituents, J. Geophys. Res., 107, 4332–4358, 2002.
Harley, R. A., Russell, A. G., McRae, G. J., Cass, G. R., and Seinfeld, J. H.: Photochemical modeling of the Southern California air quality study, Envir. Sci. Tech., 27, 378–388, 1993.
Li, S. P., Matthews, J., and Sinha, A.: Atmospheric hydroxyl radical production from electronically excited $NO_2$ and $H_2O$, Science, 319, 1657–1660, 2008.
Meng, Z., Dabdub, D., and Seinfeld, J. H.: Chemical coupling between atmospheric ozone and particulate matter, Science, 277, 116–119, 1997.
Milford, J. B., Gao, D., Sillman, S., Blossey, P., and Russell, A. G.: Total reactive nitrogen ($NO_y$) as an indicator of the sensitivity of ozone to reductions in hydrocarbon and $NO_x$ emissions, J. Geophys. Res., 99D, 3533–3542, 1994.
Nguyen, K. and Dabdub, D.: $NO_x$ and VOC control and its effect on the formation of aerosols, Aerosol Sci. Tech., 36, 560–572, 2002.
Qin, Y., Tonnesen, G. S., and Wang, Z.: Weekend/weekday differences of ozone, $NO_x$, CO, VOCs, $PM_{10}$ and the light scatter during ozone season in Southern California, Atmos. Environ., 38, 3069–3087, 2004.
Russell, A. and Dennis, R.: NARSTO critical review of photochemical models and modeling, Atmos. Environ., 34, 2283–2324, 2000.
Seinfeld, J. H. and Pandis, S. N.: Atmospheric Chemistry and Physics: From Air Pollution to Climate Change, 2nd ed., Wiley, New Jersey, pp 235–238, 2006.
Winner, A. D., Cass, G. R. and Harley, R. A.: Effect of alternative boundary conditions on predicted ozone control strategy performance: A case study in the Los Angeles area, Atmos. Environ., 29, 3451–3464, 1995.
Zeldin, M. D., Bregman, L. D., and Horie, Y. A.: Meteorological and air quality assessment of the representativeness of the 1987 SCAQS Intensive Days, Final report to the South Coast Air Quality Management District, 1990.





**Table 1.** Reaction rates for photo-excited $NO_2$ reacting with $H_2O$ are presented. High and low reaction rates correspond to the reaction rates determined experimentally by Li et al. (2008) and Crowley and Carl (1997), respectively.

| Simulated case | Reaction rate (Reaction R7) |
|---|---|
| Base case | No photo-excited $NO_2$ chemistry |
| Low reaction rate case | $1.2\times10^{-14}$ $cm^3$ $mol^{-1}$ $s^{-1}$ |
| High reaction rate case | $1.7\times10^{-13}$ $cm^3$ $mol^{-1}$ $s^{-1}$ |



ACPD
9, 18985–19008, 2009





**Table 2.** Statistical analysis of model performance by comparing measured ozone, NO, and $NO_2$ concentrations to those predicted by the UCI-CIT Airshed Model with and without $NO_2$ photo-excitation chemistry is presented. The low reaction rate case refers to utilizing the reaction rate found by Crowley and Carl (1997) for Reaction (R2). The high reaction rate case refers to utilizing the reaction rate found by Li et al. (2008) for Reaction (R2).

| | Base case (%) | Low reaction rate case (%) | High reaction rate case (%) |
|---|---|---|---|
| Ozone | | | |
| Normalized Gross Error | 46.4 | 46.3 | 45.9 |
| Normalized Bias | −4.9 | −3.8 | 1.9 |
| Maximum Unpaired Peak Prediction | 14.5 | 15.3 | 20.2 |
| Total Unpaired Peak Prediction | −145.0 | −120.0 | −8.4 |
| NO | | | |
| Normalized Gross Error | 74.4 | 74.0 | 75.1 |
| Normalized Bias | 45.5 | 44.4 | 41.4 |
| Maximum Unpaired Peak Prediction | 127.9 | 128.1 | 128.1 |
| Total Unpaired Peak Prediction | 399.3 | 384.5 | 335.3 |
| $NO_2$ | | | |
| Normalized Gross Error | 25.5 | 25.5 | 26.1 |
| Normalized Bias | −13.0 | −12.9 | −12.8 |
| Maximum Unpaired Peak Prediction | −2.0 | −1.6 | −0.8 |
| Total Unpaired Peak Prediction | −253.9 | −250.0 | −232.6 |



ACPD
9, 18985–19008, 2009



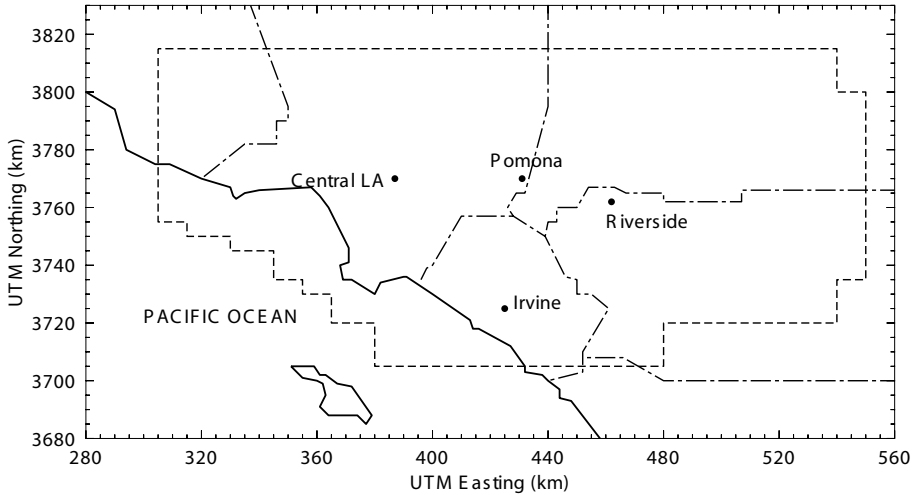


**Fig. 1.** Model domain of the UCI-CIT air quality model. The map shows the location of Central Los Angeles, Pomona, and Riverside, which are the primary locations of interest for this analysis. Measurements from additional locations (not shown) were used to perform a statistical analysis of model accuracy.



ACPD
9, 18985–19008, 2009



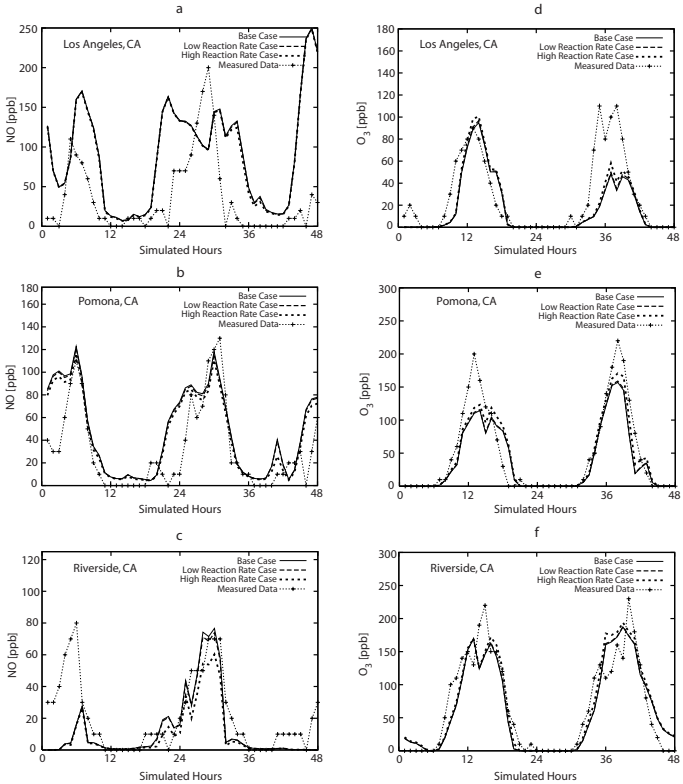


**Fig. 2.** Simulated and measured NO and ozone concentrations in the South Coast Air Basin of California for 27–28 August 1987 is presented. All figures depict four cases which include 1-h average concentrations for the UCI-CIT base case, 1-h average concentrations for a case with $NO_2$ photo-excitation chemistry utilizing the low reaction rate (Crowley and Carl, 1997), 1-h average concentrations for a case with $NO_2$ photo-excitation chemistry utilizing the high reaction rate (Li et al., 2008), and measured concentrations from the California Air Resources Board (ARB). The numerical values of the high and low reaction rates are shown in Table 1. Subfigures shown correspond to **(a)** NO in Los Angeles, **(b)** NO in Pomona, **(c)** NO in Riverside, **(d)** ozone in Los Angeles, **(e)** ozone in Pomona, and **(f)** ozone in Riverside. All concentrations are in ppb.



ACPD
9, 18985–19008, 2009



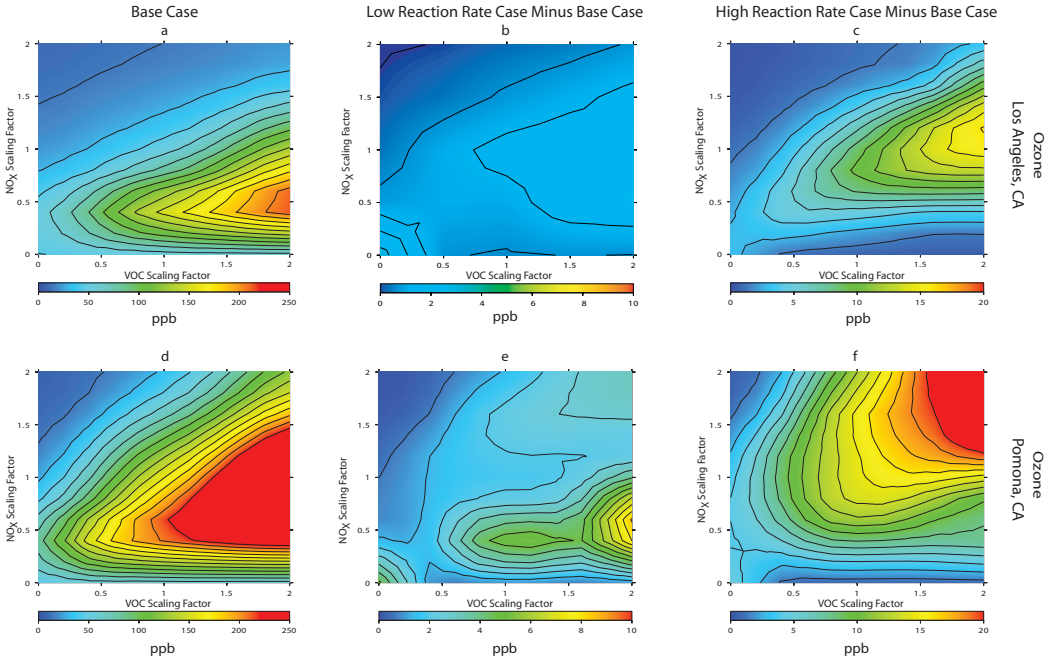


**Fig. 3.** Impact of $NO_2$ photo-excitation chemistry on ozone and $PM_{10}$ concentrations in the South Coast Air Basin of California for 28 August 1987: **(a)** Peak 1-h average ozone concentrations for base case in Los Angeles, **(b)** Peak 1-h average ozone concentrations for low reaction rate case minus those from base case in Los Angeles, **(c)** Peak 1-h average ozone concentrations for high reaction rate case minus those from base case in Los Angeles **(d)** Peak 1-h average ozone concentrations for base case in Pomona, **(e)** Peak 1-h average ozone concentrations for low reaction rate case minus those from base case in Pomona, **(f)** Peak 1-h average ozone concentrations for high reaction rate case minus those from base case in Pomona **(g)** Peak 1-h average ozone concentrations for base case in Riverside, **(h)** Peak 1-h average ozone concentrations for low reaction rate case minus those from base case in Riverside, **(i)** Peak 1-h average ozone concentrations for high reaction rate case minus those from base case in Riverside, **(j)** 24-h average $PM_{10}$ concentrations for base case in Riverside, **(k)** 24-h average $PM_{10}$ concentrations for low reaction rate case minus those from base case in Riverside, **(l)** 24-h average $PM_{10}$ concentrations for high reaction rate case minus those from base case in Riverside. High and low reaction rates correspond to reaction rates of photo-excited $NO_2$ reacting with $H_2O$ determined experimentally by Li et al. (2008) and Crowley and Carl (1997), respectively. See Table 1 for numerical values of the reaction rates.



ACPD
9, 18985–19008, 2009



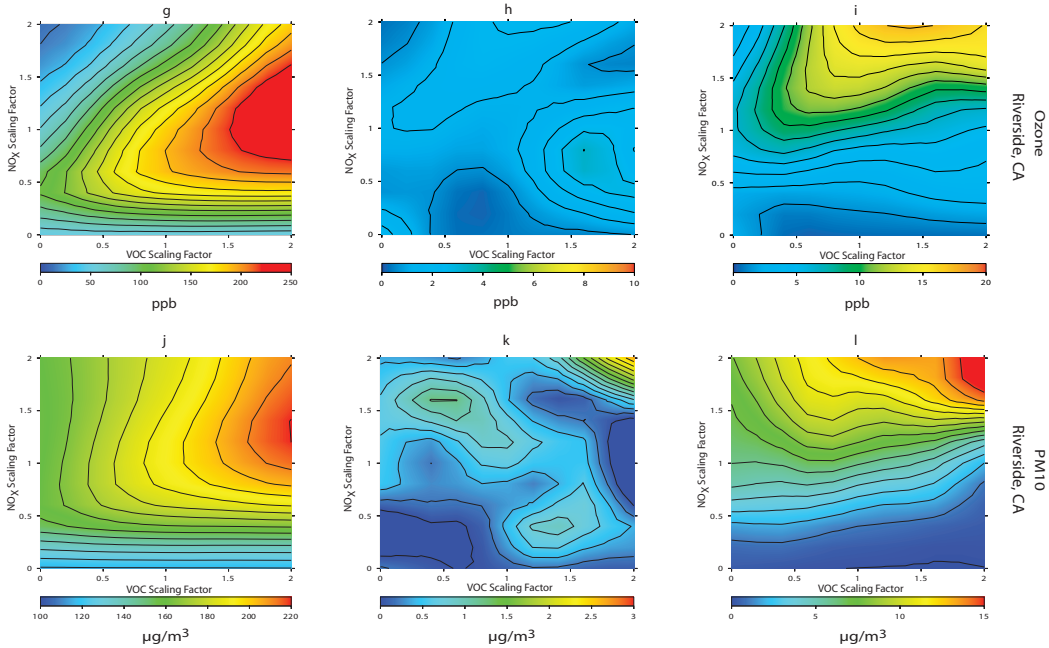


**Fig. 3.** Continued.



ACPD
9, 18985–19008, 2009